photonics

MDPI

Article

Numerical Simulation of High-Power Optical Amplifiers at 2.3 μm Based on a Special Multicore Fiber

Elena A. Anashkina *, Alexey V. Andrianov and Alexander G. Litvak

A.V. Gaponov-Grekhov Institute of Applied Physics of the Russian Academy of Sciences, 46 Ulyanov Street, 603950 Nizhny Novgorod, Russia
* Correspondence: elena.anashkina@ipfran.ru

Abstract: The development of high-power laser sources at 2.3 μm is highly demanded for remote sensing and other applications. However, this wavelength is poorly covered by present-day lasers. To obtain 100 W class high-power radiation at 2.3 μm, we propose to use simultaneously cascade laser amplification at 2 and 2.3 μm with a commercially available diode pump at 793 nm and stimulated Raman scattering between the amplified signal waves in a special zinc–tellurite multicore fiber with ten trivalent-thulium-ion-doped cores arranged in a ring. We demonstrate numerically that the use of an out-of-phase supermode (with spatial phases differing by π in neighboring cores) can provide up to 50% efficiency conversion from the 793 nm pump to the 2.3 μm wave.

Keywords: multicore fiber; tellurite glass fiber; stimulated Raman scattering (SRS); Raman gain; trivalent thulium ions; laser amplification

check for updates

Citation: Anashkina, E.A.; Andrianov, A.V.; Litvak, A.G. Numerical Simulation of High-Power Optical Amplifiers at 2.3 μm Based on a Special Multicore Fiber. *Photonics* **2023**, *10*, 711. https://doi.org/10.3390/photonics10070711

Received: 17 May 2023
Revised: 11 June 2023
Accepted: 17 June 2023
Published: 21 June 2023

Copyright: © 2023 by the authors. Licensee MDPI, Basel, Switzerland. This article is an open access article distributed under the terms and conditions of the Creative Commons Attribution (CC BY) license (https://creativecommons.org/licenses/by/4.0/).

1. Introduction

In recent years, the development of coherent light sources at a wavelength of about 2.3–2.5 μm has been attracting increasing interest [1–7]. One of the main reasons is that the earth's atmosphere is highly transparent in this spectral region. Hazardous gases such as HF, CH_4, and CO have pronounced absorption lines near 2.3 μm, which opens up an opportunity for using 2.3 μm lasers for remote sensing. In addition, laser sources at this wavelength are in demand for LiDARs and other applications. Many real applications require high power (tens of watts and even higher), which is a challenge for modern laser systems, but works in this direction are actively underway based on solid-state lasers [1–3] and fiber lasers and amplifiers [4–7]. Bulk lasers can provide higher output powers on average, but fiber lasers are generally characterized by high beam quality, alignment-free operation, and good heat dissipation. In addition, some fiber laser systems are capable of producing high average power too (~100 W and higher).

A very promising way to develop laser sources operating beyond 2.1 μm is based on using tellurite (tellurium dioxide-based) glass fibers [8]. Silica glasses commonly used for near-IR fiber devices have large losses beyond 2.1 μm, so their use is very limited at longer wavelengths (although not excluded [9]). Tellurite glasses are transparent in the range of ~0.5–5 μm, have excellent optical and physicochemical properties [8,10–13] and fairly high damage thresholds (i.e., they can resist high peak intensities [14]), can be doped with high concentrations of active ions [15], and are produced with low background losses [8]. Lasers at 2.3 μm based on tellurite fibers doped with trivalent thulium ions have been successfully demonstrated [5–7], but their experimental powers still do not exceed several hundred mW [7]. Another promising approach to generate light at 2.3 μm is to use stimulated Raman scattering (SRS) in undoped tellurite fibers pumped at 2 μm. This approach was theoretically explored in [16], where a continuous wave (CW) Raman laser with a power of ~160 W at a wavelength of 2.35 μm based on a single-mode fiber with a pump power of 300 W at 2 μm was demonstrated numerically. However, single-mode

fiber lasers at 2 μm with a power of 300 W are non-standard and rather complex devices, manufactured only in individual scientific laboratories. In addition, it remains an open question whether a single-mode tellurite fiber can resist such CW powers.

In this work, for obtaining high-power radiation at 2.3 μm in a Tm-doped tellurite multicore fiber amplifier, we propose to simultaneously use a unique combination of cascade lasing at two radiative transitions together with SRS processes. This is inherent specifically for zinc–tellurite (TZ, TeO_2–ZnO-based) glasses doped with trivalent thulium ions, which, in principle, makes it possible to obtain the efficiency of conversion of the pump at 793 nm to a signal at 2.3 μm above the Stokes limit (0.793 μm/2.3 μm = 34.5%). A simplified diagram of laser levels of trivalent thulium in a TZ glass matrix is shown in Figure 1a [15]. Previously, it was shown that the cascade scheme of dual-band operation at the $^3H_4 \rightarrow {}^3H_5$ and $^3F_4 \rightarrow {}^3H_6$ transitions with a pump wave at 793 nm can significantly increase the efficiency for a wave at 2.3 μm compared to operation only at the $^3H_4 \rightarrow {}^3H_5$ transition, since it helps to overcome the bottleneck problem related to a long lifetime of $^3F_4$ [5]. It is also known that Raman gain is very large for TZ glasses, with the maximum at about 750 cm^{-1} (22.5 THz), which is ~60 times higher than the maximum for silica glass [15]. Therefore, additional amplification of a signal at 2.3 μm due to the SRS of the wave at ~2 μm is also possible. The scheme of the SRS process is shown in Figure 1b. In this case, for the Raman amplification at 2.3 μm, the wavelength of 1.96 μm displaced by 22.5 THz is most suitable. The Raman gain of the TZ glass in comparison with the Raman gain of the silica glass is plotted in Figure 1c based on the data presented in [17]. Note that in [5], the parameters of the system were such that the SRS processes for them were negligible.

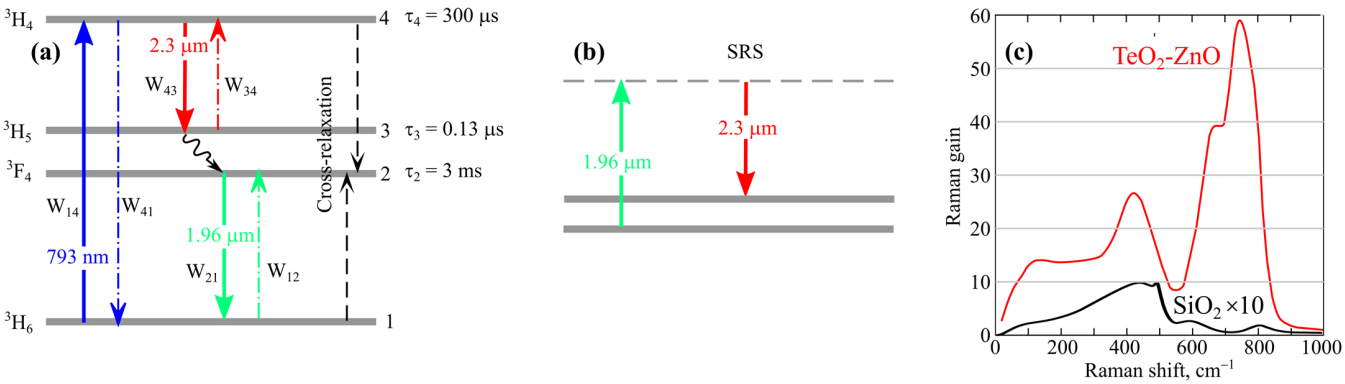

Figure 1. (**a**) Simplified diagram of the energy levels of trivalent thulium ions in the TZ glass matrix. W_{jk} are stimulated rates from level j to level k, and τ_j is the total lifetime of level j. (**b**) Schematic diagram of the SRS process. (**c**) Raman gain spectra of TZ glass (red) compared to silica glass (black; magnification by a factor of 10).

The concept of a master-oscillator power amplifier (MOPA) considered in this paper is often used for high-power laser systems [18,19]. At the same time, special fiber designs, e.g., multimode large mode area (LMA) fibers operating in quasi-single mode, are frequently developed for high-power amplifiers [18,20,21].

It is also possible to use taper fibers with a thin single-mode core at the input and a thick core at the out-put [22,23]. With adiabatic signal amplification, the output beam quality can be very high, while the scattering into higher modes is rather small. One can also use multicore fibers with N cores when each core is a single-mode one [24–26]. In the case of evanescent-field coupling, there are N supermodes in the system [25,27]. It was demonstrated that the use of an out-of-phase supermode of a multicore fiber with a symmetrical arrangement of axially symmetric cores, for which the spatial phases in neighboring cores differ by π, has a number of advantages over a "common" in-phase supermode, for which the phases are the same in all cores [28–31]. This issue was dis-cussed in detail in [28–31], here we only note that the in-phase mode is unstable at high powers, while the out-of-phase mode is stable. Moreover, it has been predicted theoretically that the self-focusing limit for the beam

power (for continuous medium) can be overcome using the out-of-phase mode, while this is impossible for the in-phase mode due to its instability [28,29]. As shown experimentally and numerically, with selective excitation of the out-of-phase supermode during amplification, the mode composition at the output does not deteriorate [30]. Moreover, the out-of-phase mode overlaps better with the doped core, so it has a higher gain (this statement will be demonstrated below). Multicore fibers can be fabricated from various glasses, including tellurite ones. A rare-earth ion-doped multicore fiber was experimentally reported in [32], and a passive seven-core tellurite fiber was demonstrated, for example, in [33]. Although the manufacture of high-quality multicore tellurite fibers is still a challenge today, in principle, technologies can be improved to the required level.

Here, we propose and numerically investigate high-power amplifiers at a wavelength of 2.3 μm based on a special double-clad TZ fiber with N = 10 step-index cores doped with trivalent thulium ions symmetrically arranged along the ring. A multicore fiber geometry leads to a decrease in peak intensities of laser beams relative to a single-mode fiber geometry and helps to prevent potential fiber damage for high-power laser amplifiers. It will be demonstrated that the use of the out-of-phase supermode is more efficient than the in-phase supermode. We propose to use a low-power seed signal at 2.3 μm and an additional low-power seed signal at ~2 μm with a standard 300 W diode pump at 793 nm. Two seeding low-power waves at 2.3 μm and 1.96 μm (with a power of about 1 mW) can be generated simultaneously in laser elements based on various matrices doped with trivalent thulium ions [5–7]. Note that at present, relatively cheap commercially available laser diodes provide powers up to several hundred watts at a wavelength of 793 nm. In this case, the efficiency of converting the pump power to a wave at 2.3 μm, as will be shown below, can reach 50% due to the combination of laser and SRS processes. The scheme of a cascade laser amplifier, with one wave used for additional amplification of another due to SRS, has not been studied before to the best of our knowledge.

2. Materials and Methods

We considered a special design of a double-clad TZ glass multicore fiber shown in Figure 2a. Ten step-index cores doped with trivalent thulium ions are arranged in a ring. The diameter of each core is d = 7 μm, and the distance between the centers of neighboring cores is $L = 1.2 \times d$ = 8.4 μm. The refractive index of the first undoped cladding is chosen to be 0.1 less than the refractive index of the core glass (Figure 2b), which can be achieved by a slight change in the content of zinc oxide in TZ glass compositions [5]. The parameters of each core are chosen so that it is single mode at signal wavelengths. A diode pump at 793 nm is launched into the first undoped cladding, which has a diameter of D = 200 μm. This diameter D coincides with the typical diameter of the fiber core, which outputs a diode pump with a power of hundreds of watts. In this case, the numerical aperture between undoped cladding and cladding 2 of the TZ multicore fiber should correspond to the numerical aperture of the fiber that outputs the pump (typically NA = 0.22). The multicore fiber also has the second cladding (its diameter is not important in the calculations).

We found supermode structures for the special multicore TZ fiber using finite element modeling, as in our previous work [34]. Figure 3 shows examples of all ten supermodes calculated at a wavelength of 1.96 μm. Mode 1 (in-phase supermode) has the highest effective refractive index, and mode 10 (out-of-phase supermode) has the lowest effective refractive index. The pair of modes 2 and 3 is degenerate in the effective refractive index. The pairs of modes 4, 5 as well as 6, 7, and 8, 9 are also degenerate. The in-phase and out-of-phase supermodes have the most symmetrical structures. For them, $|E_x|$ distributions are the same for each core. For other modes, $|E_x|$ distributions are not the same in different cores; moreover, in some cores, the fields are close to zero or small. Therefore, for modes 2–9, the gain coefficients provided by trivalent thulium ions are obviously lower due to the smaller overlap with the doped region than for modes 1 and 10. Moreover, the preparation of seed signals for amplifiers in modes 2–9 is more difficult than in modes 1 and 10. In-phase and out-of-phase supermodes can be prepared using, for example, a

special beam shaper (systems based on spatial light modulators are commonly used for such purposes) [30,35]. Further, we consider only in-phase and out-of-phase modes.

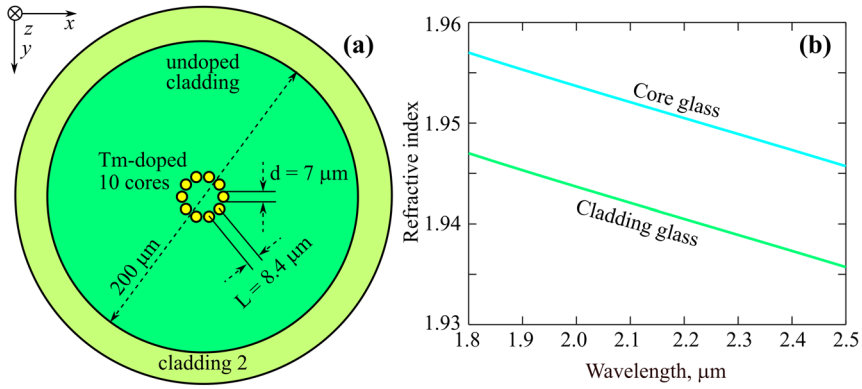

Figure 2. (**a**) Cross section of the proposed multicore TZ glass fiber with trivalent thulium-doped cores. (**b**) Wavelength-dependent refractive indexes for core and cladding TZ glasses.

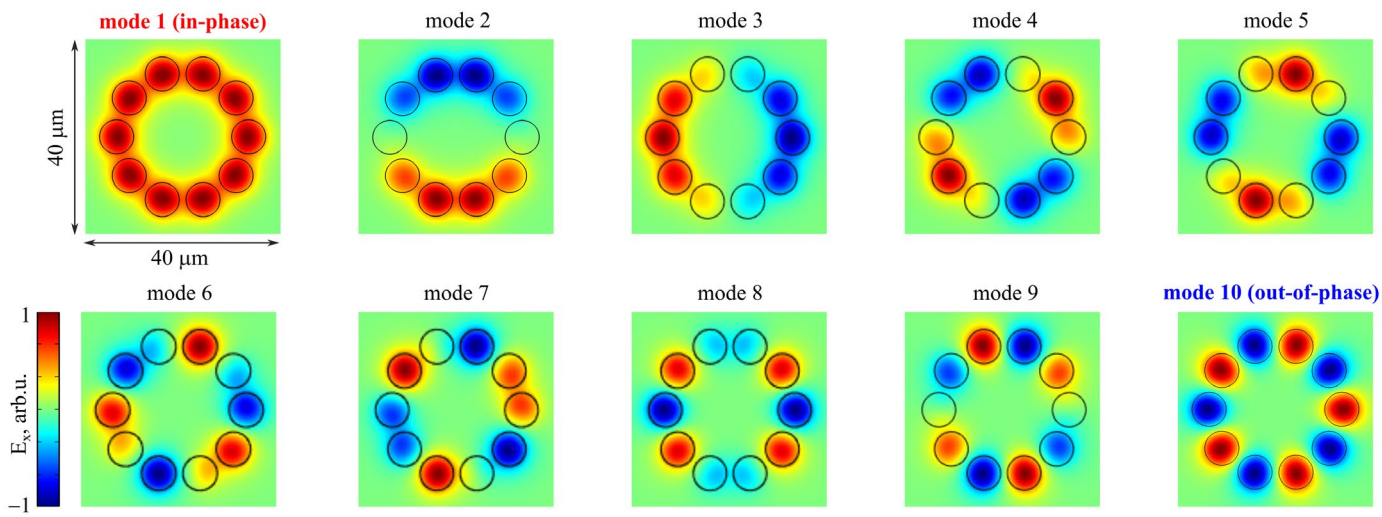

Figure 3. Calculated distributions of x-components of electric fields for supermodes at 1.96 μm. The lowest supermode (mode 1) is in-phase one. The highest supermode (mode 10) is out-of-phase one.

We calculated effective mode areas for in-phase and out-of-phase supermodes as functions of wavelength. The results are plotted in Figure 4. The mode spatial structures at 1.96 μm and 2.3 μm which are of primary interest are shown in the insets in Figure 4.

Effective supermode areas are calculated as

$$A_{eff} = \frac{\left(\int S_z dxdy\right)^2}{S_z^2 dxdy}, \tag{1}$$

where S_z is the z-component of the Poynting vector.

A schematic diagram of the considered multicore fiber laser amplifier seeded by a dual-wavelength source at 1.96 μm and 2.3 μm with a high-power diode pump at 793 nm is shown in Figure 5. To excite a required supermode, a beam shaper, for example, based on a spatial light modulator can be used [30].

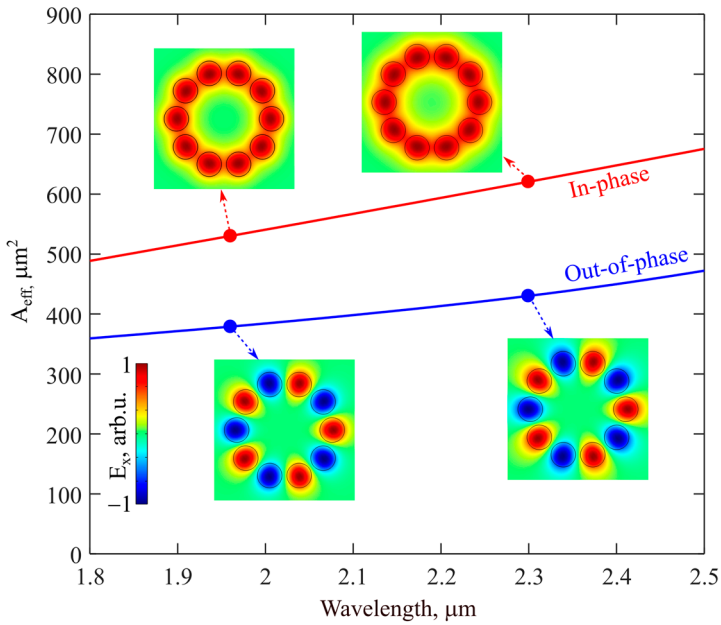

Figure 4. Wavelength-dependent effective mode areas for in-phase and out-of-phase supermodes. Insets show the corresponding distributions of x-components of electric fields E_x at 1.96 μm and 2.3 μm.

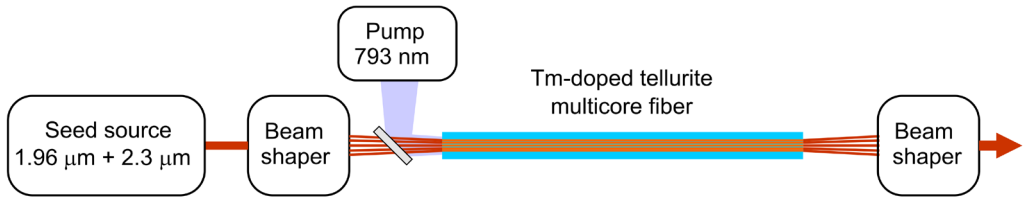

Figure 5. Schematic diagram of the laser amplifier based on Tm-doped tellurite multicore fiber.

To simulate a dual-wavelength laser amplifier with allowance for the SRS process between waves at 1.96 and 2.3 μm, we generalized the system of rate equations and the power evolution equations presented in [5,15]. The SRS was considered in a standard way [27]. We analyzed CW waves, but this model can be valid for describing pulsed amplifiers with signal durations noticeable longer than the total lifetime of level $^3F_4$. In this case, all powers refer to peak values. This approach may be justified when average powers should be reduced. The rate equations for the population densities n_1, n_2, n_3, and n_4 (normalized to the concentration of trivalent thulium ions N_{Tm}) in the steady state are [5,15]:

$$n_1 + n_2 + n_3 + n_4 = 1 \tag{2}$$

$$\frac{\partial n_4}{\partial t} = W_{14}n_1 + W_{34}n_3 - \left(W_{41} + W_{43} + \frac{1}{\tau_4}\right)n_4 - K_{CR}n_4n_1 = 0 \tag{3}$$

$$\frac{\partial n_3}{\partial t} = -\left(W_{34} + \frac{1}{\tau_3}\right)n_3 + \left(W_{43} + \frac{\beta_{43}}{\tau_4^R} + \frac{1}{\tau_4^{NR}}\right)n_4 = 0 \tag{4}$$

$$\frac{\partial n_2}{\partial t} = W_{12}n_1 - \left(W_{21} + \frac{1}{\tau_2}\right)n_2 + \frac{n_3}{\tau_3} + \frac{\beta_{42}}{\tau_4^R}n_4 + 2K_{CR}n_4n_1 = 0, \tag{5}$$

where t is time, τ_j is the total lifetime of level j, ${\tau_4}^R$ and ${\tau_4}^{NR}$ are the radiative and non-radiative lifetimes of level 4, W_{jk} are the stimulated rates from level j to level k, β_{4j} is the

branching ratio from level 4 to level j, and K_{CR} is the cross-relaxation rate (see the scheme in Figure 1a) [5,15]. Stimulated absorption and emission rates for a pump wave are:

$$W_{14,41} = \frac{\Gamma_p \lambda_p \sigma_{14,41} P_p}{hcA_{doped}} \tag{6}$$

where c is the speed of light, h is the Planck's constant, σ_{14} and σ_{41} are the absorption and emission cross sections at a pump wavelength λ_p, P_p is the wave power, A_{doped} is the area of doped cores, and Γ_p is the overlap integral of the pump intensity distribution with the doped regions estimated as $\Gamma_p = A_{doped}/(\pi D^2/4)$. Stimulated emission and absorption rates for signal waves at λ_1 = 1.96 µm and λ_2 = 2.3 µm with powers P_1 and P_2, respectively, are:

$$W_{21,12} = \frac{\Gamma_1 \lambda_1 \sigma_{21,12} P_1}{hcA_{doped}} \tag{7}$$

$$W_{43,34} = \frac{\Gamma_2 \lambda_2 \sigma_{43,34} P_2}{hcA_{doped}}, \tag{8}$$

where $\Gamma_{1,2}$ are the overlap integrals of the signal waves with the doped regions.

The SRS-modified equations for the power evolution along the z-axis are:

$$\frac{dP_p}{dz} = -\Gamma_p N_{Tm}(\sigma_{14} n_1 - \sigma_{41} n_4) P_p - \alpha_p P_p \tag{9}$$

$$\frac{dP_1}{dz} = \Gamma_1 N_{Tm}(\sigma_{21} n_2 - \sigma_{12} n_1) P_1 - g_{R12} \frac{\lambda_2}{\lambda_1} P_2 P_1 - \alpha_1 P_1 \tag{10}$$

$$\frac{dP_2}{dz} = \Gamma_2 N_{Tm}(\sigma_{43} n_4 - \sigma_{34} n_3) P_2 + g_{R12} P_1 P_2 - \alpha_2 P_2 \tag{11}$$

where α_1, α_2, and α_p are the linear losses at wavelengths λ_1, λ_2, and λ_p, respectively; g_{R12} is the Raman gain coefficient for the TZ fiber calculated as

$$g_{R12} = \frac{g_R(\text{TZ@1µm}) \times (1\text{µm}/\lambda_1)}{\left(A_{eff1} + A_{eff2}\right)/2} \tag{12}$$

Here, g_R(TZ@1µm) is the maximum Raman gain for bulk TZ glass for the pump wave at 1 µm [17,27]. For most of the simulations, we set optical losses of 0.3 dB/km for laser waves, which is easily achievable for modern single-core tellurite fibers and, in principle, can be achieved for multicore tellurite fibers. At the very end of the section Results, we will also analyze the impact of higher losses (up to 5 dB/m) that can be caused by light scattering at the core-cladding interfaces, bending losses, and so on.

The system of Equations (9)–(11), with allowance for the rate Equations (2)–(5) in the steady state, was solved numerically by the classical Runge–Kutta method (with adaptive step size). The used parameters are listed in Table 1. We neglected the spontaneous Raman scattering to the anti-Stokes wave and the second-order Raman scattering to the Stokes wave. At room temperature, the process of scattering to the anti-Stokes component is weak. Moreover, its expected wavelength of 1.7 µm is strongly absorbed by Tm ions. The 2nd order Stokes Raman wave at the expected wavelength of about 2.8 µm is strongly absorbed by hydroxyl groups in zinc–tellurite glass.

Table 1. Parameters used in simulation.

Parameter	Symbol	Value
Core diameter	d	7 μm
Distance between centers of neighboring cores	L	8.4 μm
Number of cores	N	10
Cladding diameter	D	200 μm
Pump wavelength	λ_p	793 nm
Wavelength at $^3F_4 \rightarrow {}^3H_6$ transition	λ_1	1.96 μm
Wavelength at $^3H_4 \rightarrow {}^3H_5$ transition	λ_2	2.3 μm
Effective supermode area at 1.96 μm	A_{eff1}	530 μm^2 (in-phase) 380 μm^2 (out-of-phase)
Effective supermode area at 2.3 μm	A_{eff2}	620 μm^2 (in-phase) 430 μm^2 (out-of-phase)
Overlap integral (pump with doped area)	Γ_p	0.012
Overlap integral (wave at 1.96 μm with doped area)	Γ_1	0.73 (in-phase) 0.95 (out-of-phase)
Overlap integral (wave at 2.3 μm with doped area)	Γ_2	0.62 (in-phase) 0.9 (out-of-phase)
Fiber loss at 793 nm	α_p	0.4 dB/m
Fiber loss at 1.96 μm	α_1	0.3 dB/m (Figures 6–9) 0.3–5 dB/m (Figure 10)
Fiber loss at 2.3 μm	α_2	0.3 dB/m
Raman gain of bulk TZ glass at 1 μm	g_R(TZ@1 μm)	59×10^{-13} m/W
Raman gain coefficient (for wave at 2.3 μm amplified by wave at 1.96 μm)	g_{R12}	7.3×10^{-5} (W cm)$^{-1}$ (in-phase) 5.1×10^{-5} (W cm)$^{-1}$ (out-of-phase)
Absorption cross section at $^3H_6 \rightarrow {}^3H_4$	σ_{14}	1×10^{-24} m^2
Emission cross section at $^3H_4 \rightarrow {}^3H_6$	σ_{41}	1×10^{-24} m^2
Emission cross section at $^3F_4 \rightarrow {}^3H_6$	σ_{21}	2.6×10^{-25} m^2
Absorption cross section at $^3H_6 \rightarrow {}^3F_4$	σ_{12}	1.2×10^{-26} m^2
Emission cross section at $^3H_4 \rightarrow {}^3H_5$	σ_{43}	2.6×10^{-25} m^2
Absorption cross section at $^3H_5 \rightarrow {}^3H_4$	σ_{34}	2.6×10^{-25} m^2
Total lifetime of level $^3H_6$	τ_4	300 μs
Radiative lifetime of level $^3H_6$	${\tau_4}^R$	400 μs
Non-radiative lifetime of level $^3H_6$	${\tau_4}^{NR}$	1.2 ms
Total (non-radiative) lifetime of level $^3H_5$	τ_3	0.13 μs
Total lifetime of level $^3F_4$	τ_2	3 ms
Branching ratio from level 4 ($^3H_6$) to level j	β_{41} β_{42} β_{43}	0.9 0.07 0.03
Cross-relaxation rate	K_{CR}	1262 s^{-1} (for $N_{Tm} = 1 \times 10^{20}$ cm^{-3}) 5678 s^{-1} (for $N_{Tm} = 2 \times 10^{20}$ cm^{-3}) 31,068 s^{-1} (for $N_{Tm} = 4 \times 10^{20}$ cm^{-3}) 164,370 s^{-1} (for $N_{Tm} = 8 \times 10^{20}$ cm^{-3})

3. Results

Let us first revisit the main idea of the paper: in high-power dual-wavelength fiber amplifiers based on a special TZ fiber doped with trivalent thulium ions, the interaction between waves at 1.96 μm and 2.3 μm due to SRS leads to a significant increase in the efficiency of power conversion from the diode pump at 793 nm to the wave at 2.3 μm. Moreover, the conversion efficiency is higher for the out-of-phase supermode than for the in-phase one because the effective area of the out-of-phase supermode is smaller than

that of the in-phase one (for example, the effective mode area is 430 μm^2 for out-of-phase and 620 μm^2 for in-phase supermodes at 2.3 μm); the out-of-phase supermode is better localized near the cores. This is due to the fact that the topological structures of the field distributions of in-phase and out-of-phase modes are different. There are lines of zero field amplitude between the cores for the out-of-phase mode (due to equal amplitudes and phase difference by π at these lines), so most of its power is contained in the cores. On the contrary, there is significant field amplitude in the regions between the cores for the in-phase mode, as clearly seen in Figure 4. The overlap integrals with doped cores for the out-of-phase supermode are higher (see Table 1); hence, the laser gain coefficients are higher too. In addition, the Raman gain is also higher for the out-of-phase supermode (see Table 1).

Figure 6 (left column) shows the results of calculations performed for the out-of-phase supermode, and Figure 6 (right column) for the in-phase one. Hereinafter, the seed signal powers at 1.96 μm and at 2.3 mW are 10 mW and 1 mW, respectively. We checked that the exact values of low-power seed signals do not affect the output powers of 100-W class signals. The pump power was 200 W, and the concentration of active ions was $N_{Tm} = 4 \times 10^{20}$ cm^{-3}. We purposely switched on and off the SRS in the calculations to reveal its contribution. The results obtained for the complete model are plotted as solid curves and for the model without SRS as dashed curves. Figure 6a,b show the evolution of the wave power at 2.3 μm, and Figure 6c,d at 1.96 μm; whereas Figure 6e,f show the evolution of the pump wave power.

At short distances from the fiber input end, there is cascading laser amplification of both signal waves, and the contribution of the SRS is small. The SRS effect becomes significant when the power in the wave at 1.96 μm is sufficiently large and almost reaches its maximum. This occurs approximately when most of the pump power has been absorbed (vertical line through Figure 6a,c,e). After that, the wave at 1.96 μm ceases to be amplified. In the complete model with SRS, the power is further efficiently transferred from the wave at 1.96 μm to the wave at 2.3 μm. In the model without SRS, the powers in both signal waves reach a maximum at close points z and then decay due to losses; there is no further interaction between them. The wave at 1.96 μm decays faster since it is partially absorbed from the ground state (at the $^3H_6 \rightarrow {}^3F_4$ transition). The wave at 2.3 μm is not absorbed at the $^3H_6 \rightarrow {}^3F_4$ transition. At practically zero pump powers, the levels above $^3F_4$ are not populated; therefore, the wave at 2.3 μm cannot be absorbed from excited states. Note that the power distribution in the pump wave is practically the same both in the model with and without SRS. In the case with allowance for SRS, the maximum power at 2.3 μm is 86 W in the out-of-phase supermode and 66 W in the in-phase one. For the out-of-phase supermode, the diode pump power conversion efficiency is 43%, exceeding the Stokes limit of 34.5%. Further study and optimization allowed us to find parameters of the system for which it is possible to achieve higher values of powers and conversion efficiencies.

Next, we studied the dependence of the power in two signal waves on two variables: the diode pump power and the fiber length for out-of-phase (Figure 7, left-hand panels) and in-phase (Figure 7, right-hand panels) supermodes with and without SRS (at $N_{Tm} = 4 \times 10^{20}$ cm^{-3}). The power curves at 2.3 μm are plotted in the top row (Figure 7a–d) and at 1.96 μm in the bottom row (Figure 7e–h).

It can be seen that at pump power < 100 W, the wave at 2.3 μm is weakly amplified, while the wave at 1.96 μm is significantly enhanced. This is explained by the cross-relaxation effect, which is rather strong at the chosen concentration of active ions. Its action leads to a decrease in the population at the $^3H_4$ level and a decrease in the laser gain at the $^3H_4 \rightarrow {}^3H_5$ transition, as well as an increase in the population at the $^3F_4$ level and a significant increase in the laser gain at the $^3H_4 \rightarrow {}^3H_6$ transition. Thus, at a pump power of 100 W, the maximum wave power at 1.96 μm is 60 W (the conversion efficiency reaches 60%) in the out-of-phase mode, which significantly exceeds its Stokes limit (0.793/1.96 = 40%). In this case, the red dashed-dotted curves in the lower panels demonstrate the optimal lengths of the wave at 1.96 μm depending on the pump power

(i.e., the z value at which the maximum P_1 is reached at a certain P_p). These dependences are rather weak and are determined by the pump absorption length, which changes weakly for the considered parameters. The blue-dotted curves in all plots show the optimal fiber lengths for maximizing wave power at 2.3 μm as a function of pump power (i.e., the z value at which P_2 is maximized at a certain P_p).

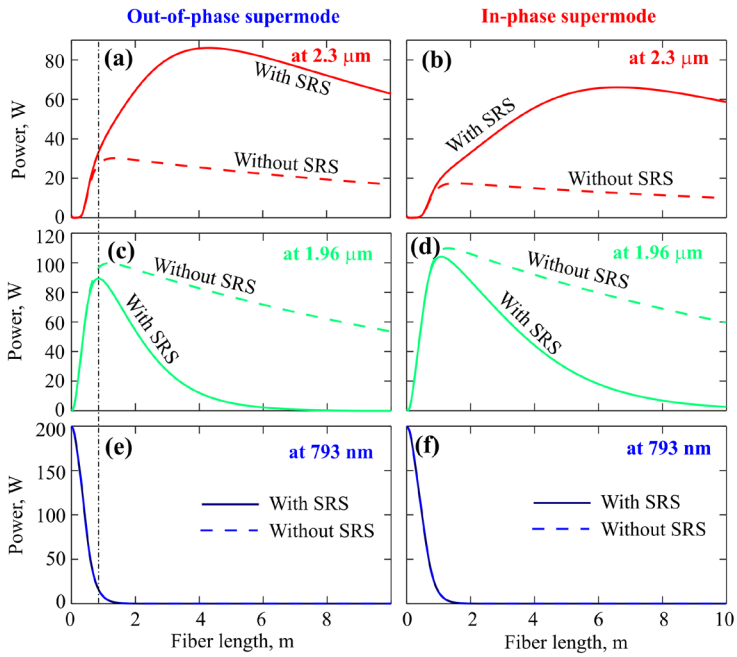

Figure 6. Powers vs. fiber length calculated with/without SRS for pump power 200 W and N_{Tm} = 4 × 10^{20} cm^{-3} for waves at 2.3 μm propagating in out-of-phase (**a**) or in-phase (**b**) supermodes; for waves at 1.96 μm in out-of-phase (**c**) or in-phase (**d**) supermodes; and for waves at 793 nm in out-of-phase (**e**) or in-phase (**f**) supermodes. The vertical dash-dotted line through Figures (**a**,**c**,**e**) shows the fiber length at which the power in the wave at 1.96 μm reaches its maximum.

In the case of switching off the SRS process, the optimal lengths are quite close for both waves since amplification occurs only due to cascade laser processes, which cease when the pump is absorbed. In the case of an allowance for SRS, the optimal lengths maximizing wave power at 2.3 μm strongly depend on the pump power. The higher the pump power, the shorter the optimal length. This has a very simple explanation: the higher the pump power, the higher the power in the wave at 1.96 μm, which means that the faster it amplifies the wave at 2.3 μm due to SRS. The optimal length for a wave at 2.3 μm is reached when the gain becomes equal to the optical loss. With the chosen TZ fiber parameters, this occurs for P_1 = 9.5 W for the out-of-phase mode and P_1 = 13.5 W for the in-phase mode (i.e., the blue-dotted curves in Figure 7e,g show the level lines corresponding to these values). In addition, as P_p increases, the population of the $^3H_6$ level increases, and the laser effects are also enhanced for the wave at 2.3 μm. At any pump power, the maximum power achieved in the wave at 2.3 μm is higher for the out-of-phase supermode than for the in-phase one.

Next, we made optimizations for the wave at 2.3 μm for various concentrations of active ions. The ratio of the power in this wave to the pump power (P_2/P_p) as a function of two variables, pump power and fiber length, is presented in Figure 8.

The following features are visible here: At low concentrations of trivalent thulium ions, amplification of the wave at 2.3 μm with a noticeable efficiency (>10%) begins at a pump power of about 10 W (Figure 8a), while with increasing concentration, a higher pump power is required (Figure 8b–d). At the highest considered value of N_{Tm}, the cross-relaxation is so strong that the laser amplification of the wave at 2.3 μm is small, and notable values of its power are achieved mainly due to the SRS process at high

powers and long fiber lengths (Figure 8d). The optimum for P_2 is achieved at intermediate concentrations of N_{Tm} =24 × 10^{20} cm^{-3} at high pump power (P_p > 150 W) (Figure 8b,c). In this case, both effects are important: laser amplification and SRS. The maximum conversion efficiency reaches 50%, which exceeds the Stokes limit by 15%.

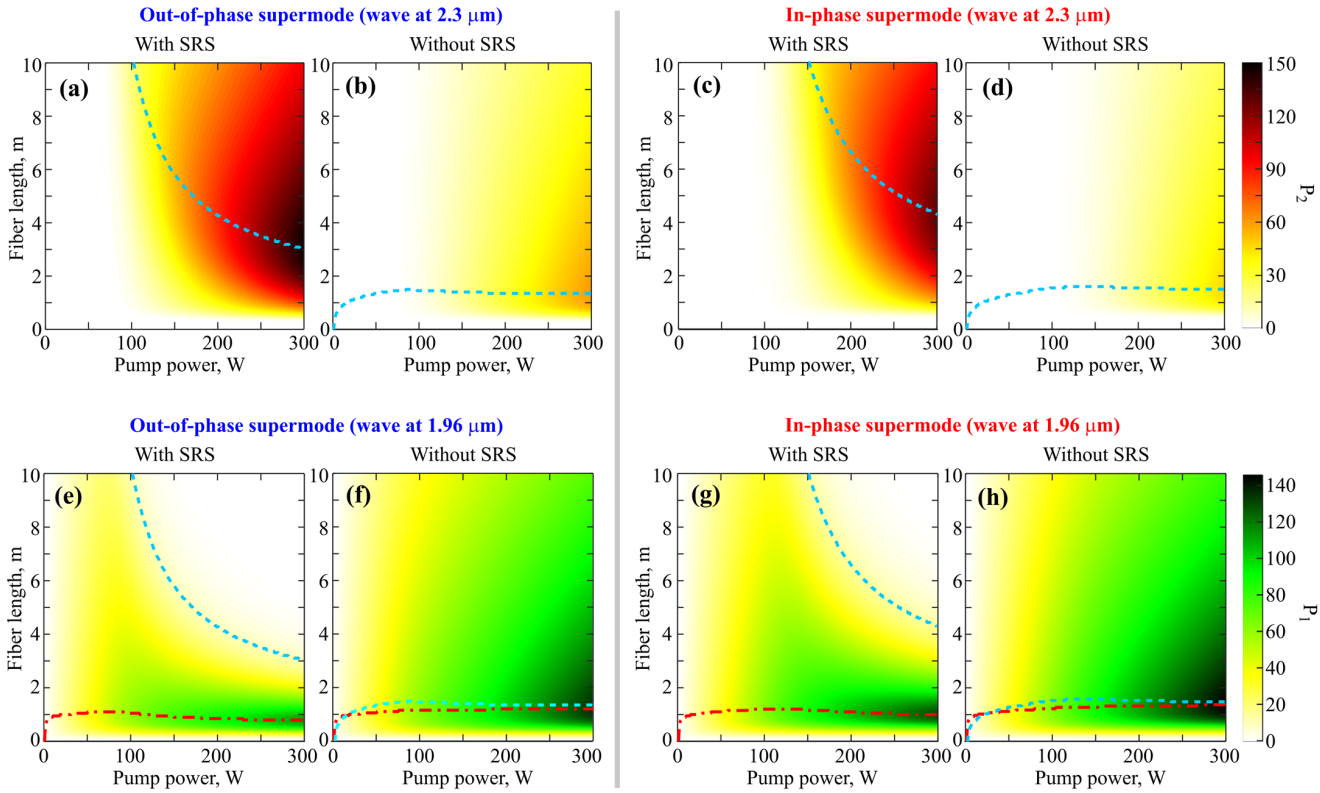

Figure 7. (**a**) Power in the wave at 2.3 μm vs. two variables: pump power and fiber length calculated for out-of-phase mode with SRS (**a**); out-of-phase mode without SRS (**b**); in-phase mode with SRS (**c**); in-phase mode without SRS (**d**). Power in the wave at 1.96 μm vs. pump power and fiber length calculated for out-of-phase mode with SRS (**e**); out-of-phase mode without SRS (**f**); in-phase mode with SRS (**g**); in-phase mode without SRS (**h**). Dotted blue curves in all panels demonstrate the optimal fiber length maximizing P_2 for certain pump power. Dash-dotted red curves in (**e**–**h**) correspond to the fiber lengths maximizing P_1 for certain pump powers.

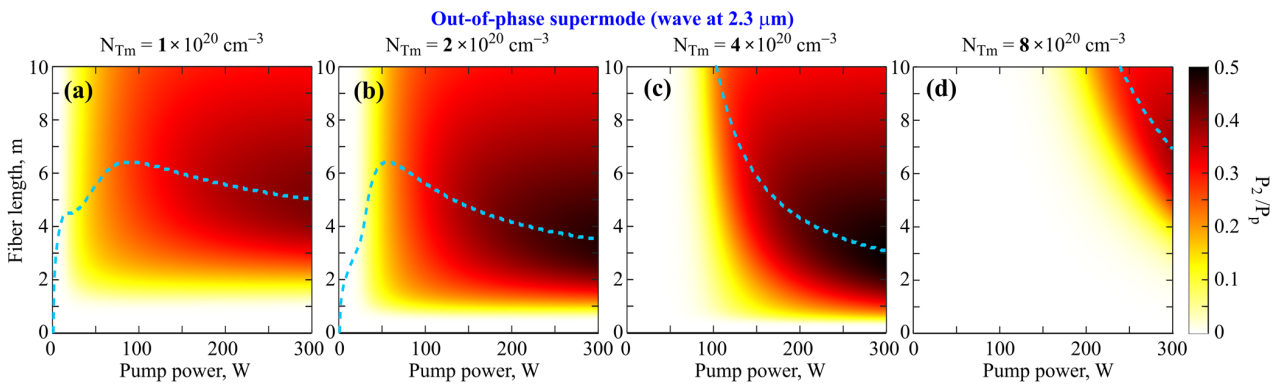

Figure 8. (**a**) Ratio of the power in the wave at 2.3 μm to the pump power (P_2/P_p) as a function of two variables: pump power and fiber length calculated for N_{Tm} = 1 × 10^{20} cm^{-3} (**a**); N_{Tm} = 2 × 10^{20} cm^{-3} (**b**); N_{Tm} = 4 × 10^{20} cm^{-3} (**c**); and N_{Tm} = 8 × 10^{20} cm^{-3} (**d**). Dotted blue curves in all panels demonstrate the optimal fiber length maximizing P_2 for certain pump power.

Next, for clarity, we plotted the dependence of the wave power at 2.3 μm on the pump power for optimal concentrations: $N_{Tm} = 2 \times 10^{20}$ cm^{-3} (Figure 9a) and $N_{Tm} = 4 \times 10^{20}$ cm^{-3} (Figure 9b). Each curve in Figure 9a,b corresponds to a certain length L = 1, 2, . . . , 7 m and, in fact, reproduces the data from Figure 8b,c. It is clearly seen that at the most optimal lengths of 3–4 m and at high powers (>150 W), these dependences are close to linear functions.

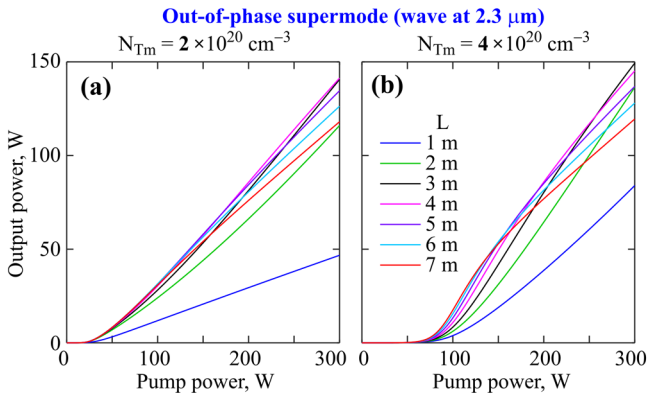

Figure 9. Power in the wave at 2.3 μm as a function of pump power for $N_{Tm} = 2 \times 10^{20}$ cm^{-3} (**a**) and $N_{Tm} = 4 \times 10^{20}$ cm^{-3} (**b**) calculated for different fiber lengths. The legend in (**b**) is shared for both panels.

Finally, we studied the effect of increased fiber losses on the quantitative characteristics of laser amplifiers. For all simulations presented above, we set optimistic losses of 0.4 dB/m at 793 nm and 0.3 dB/m at 1.96 and 2.3 μm. Here, we purposely increased losses at laser wavelengths to take into account additional imperfections (including bending losses). The simulated output powers at 2.3 μm vs. the fiber length for optimal concentration $N_{Tm} = 4 \times 10^{20}$ cm^{-3} calculated for out-of-phase supermodes with SRS and without SRS are plotted in Figure 10a,b, respectively, for different losses in the 0.3–5 dB/m range. It is not surprising that the higher the loss, the lower the output power and the shorter the optimal fiber length. More interesting is that the relative contribution of the Raman gain is much higher for relatively low losses. Comparing Figure 10a,b, it can be seen that at losses up to 2 dB/m, the output power with SRS is significantly higher than without it, while at losses ≥3 dB/m, the Raman contribution becomes relatively small. Therefore, for the experimental implementation of the proposed amplifier, one should aim to manufacture a high-quality multicore tellurite fiber.

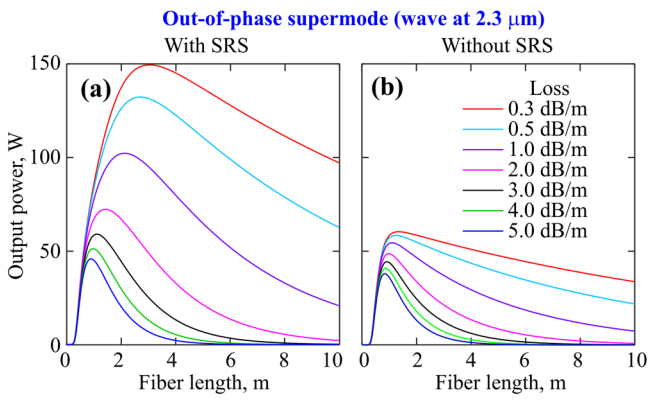

Figure 10. Powers vs. fiber length calculated with SRS (**a**) and without SRS (**b**) for waves at 2.3 μm propagating in out-of-phase supermode for pump power of 300 W and $N_{Tm} = 4 \times 10^{20}$ cm^{-3} and for different fiber losses. The legend in (**b**) is shared for both panels.

4. Discussion and Conclusions

To conclude, we have shown numerically that a trivalent-thulium-ion-doped TZ multi-core fiber with coupled axially symmetrical cores arranged in a symmetrical ring structure is a promising solution for diode-pumped optical amplifiers of 100-W power class at 2.3 µm, which is required for important applications. We studied the use of dual-wavelength seed signals with a power of order 1 mW at 1.96 µm and 2.3 µm and a commercially available diode pump at 793 nm with a power of up to 300 W. We demonstrated the possibility of attaining up to 50% conversion efficiency from the pump power to the wave at 2.3 µm which exceeds the Stokes limit by 15% due to a combination of laser amplification and SRS between signal waves (for losses of 0.3 dB/m). The proposed scheme can provide significantly higher efficiency in comparison to trivalent-thulium-ion-doped fiber lasers and amplifiers that do not benefit from additional Raman energy transfer [4–7]. Note that the use of a fiber based on TZ glass is substantial, since its Raman shift of 22.5 THz coincides with the difference in the frequencies for two different radiative transitions of the trivalent thulium ion. For other glasses that are transparent in this range, the Raman shift is smaller (~17 THz for ZBLAN [36], 10 THz for arsenic [37], ~7 THz for arsenic triselenide [37]), which is not suitable for implementing the concept of combining cascade laser amplification and SRS. We emphasize that the use of the out-of-phase supermode is important since its overlap integral with doped cores is higher compared to the commonly used in-phase supermode, whereas the out-of-phase supermode provides a higher total gain. In addition, it was previously shown that the out-of-phase supermode is stable at high powers, while the in-phase one is unstable [28–30]. As was shown in [30], small perturbations of the ideal transverse fiber structure led to a slight deformation of the out-of-phase mode, but do not lead to qualitative changes. Therefore, when deviating from the ideal geometry, only minor quantitative changes in the amplifier parameters are expected.

Note that the proposed design is especially good for high pump powers > 150 W. It provides high total power with an allowable load on each core. In this case, all powers refer to peak values. At lower target peak powers, a similar optimization can be performed using fewer cores, thereby reducing the effective mode area and increasing the Raman gain. One can also use a smaller cladding diameter to increase the overlap integral of the pump with doped cores. We considered CW waves, but the developed approach is valid for pulsed amplifiers with signal durations notably longer than the total lifetime of level $^3F_4$ (3 ms).

Author Contributions: Conceptualization, E.A.A.; methodology, E.A.A.; software, E.A.A.; validation, E.A.A. and A.V.A.; formal analysis, E.A.A. and A.V.A.; investigation, E.A.A.; data curation, E.A.A.; writing—original draft preparation, E.A.A.; writing—review and editing, A.V.A. and A.G.L.; visualization, E.A.A.; supervision, A.G.L.; funding acquisition, A.G.L. All authors have read and agreed to the published version of the manuscript.

Funding: This research was funded by the Russian Science Foundation, grant no. 23-12-00248 (https://rscf.ru/en/project/23-12-00248/ (accessed on 16 June 2023)).

Institutional Review Board Statement: Not applicable.

Informed Consent Statement: Not applicable.

Data Availability Statement: The data underlying the results presented in this article may be obtained from the authors upon reasonable request.

Conflicts of Interest: The authors declare no conflict of interest.

References

1. Moskalev, I.; Mirov, S.; Mirov, M.; Vasilyev, S.; Smolski, V.; Zakrevskiy, A.; Gapontsev, V. 140 W Cr:ZnSe Laser System. *Opt. Express* **2016**, *24*, 21090–21104. [CrossRef] [PubMed]
2. Zha, F.; Yu, X.; Chu, H.; Pan, H.; Zhao, S.; Loiko, P.; Pan, Z.; Li, D. Compact Diode-Pumped Continuous Wave and Passively Q Switched Tm:YAG Laser at 2.33 µm. *Opt. Lett.* **2022**, *47*, 6265–6268. [CrossRef] [PubMed]

3. Loiko, P.; Camy, P.; Soulard, R.; Guillemot, L.; Brasse, G.; Doualan, J.-L.; Braud, A.; Tyazhev, A.; Hideur, A.; Druon, F. Efficient Tm:LiYF4 Lasers at ∼2.3 µm: Effect of Energy-Transfer Upconversion. *IEEE J. Quantum Electron.* **2019**, *55*, 1700212. [CrossRef]
4. Li, X.; Zhu, X.; Yang, L.; Cui, Y.; Zhou, Z.; Wang, M.; Wang, Z. High-Gain Single-Frequency Tm3+-Doped ZBLAN Fiber Amplifier at 2.33 µm. *Opt. Lett.* **2023**, *48*, 502–505. [CrossRef] [PubMed]
5. Muravyev, S.V.; Anashkina, E.A.; Andrianov, A.V.; Dorofeev, V.V.; Motorin, S.E.; Koptev, M.Y.; Kim, A.V. Dual-Band Tm^{3+}-Doped Tellurite Fiber Amplifier and Laser at 1.9 µm and 2.3 µm. *Sci. Rep.* **2018**, *8*, 16164. [CrossRef]
6. Denker, B.I.; Dorofeev, V.V.; Galagan, B.I.; Koltashev, V.V.; Motorin, S.E.; Plotnichenko, V.G.; Sverchkov, S.E. 2.3 µm Laser Action in Tm^{3+}-Doped Tellurite Glass Fiber. *Laser Phys. Lett.* **2018**, *16*, 015101. [CrossRef]
7. Denker, B.I.; Dorofeev, V.V.; Galagan, B.I.; Koltashev, V.V.; Motorin, S.E.; Plotnichenko, V.G.; Sverchkov, S.E. A 200 mW, 2.3 µm Tm3+-Doped Tellurite Glass Fiber Laser. *Laser Phys. Lett.* **2020**, *17*, 095101. [CrossRef]
8. Tao, G.; Ebendorff-Heidepriem, H.; Stolyarov, A.M.; Danto, S.; Badding, J.V.; Fink, Y.; Ballato, J.; Abouraddy, A.F. Infrared fibers. *Adv. Opt. Photonics* **2015**, *7*, 379–458. [CrossRef]
9. Bufetov, I.A.; Kosolapov, A.F.; Pryamikov, A.D.; Gladyshev, A.V.; Kolyadin, A.N.; Krylov, A.A.; Yatsenko, Y.P.; Biriukov, A.S. Revolver Hollow Core Optical Fibers. *Fibers* **2018**, *6*, 39. [CrossRef]
10. Dorofeev, V.V.; Moiseev, A.N.; Churbanov, M.F.; Kotereva, T.V.; Chilyasov, A.V.; Kraev, I.A.; Pimenov, V.G.; Ketkova, L.A.; Dianov, E.M.; Plotnichenko, V.G.; et al. Production and Properties of High Purity $TeO_2-WO_3-(La_2O_3, Bi_2O_3)$ and $TeO2-ZnO-Na_2O-Bi_2O_3$ Glasses. *J. Non-Cryst. Solids* **2011**, *357*, 2366–2370. [CrossRef]
11. Linganna, K.; In, J.-H.; Kim, S.H.; Han, K.; Choi, J.H. Engineering of TeO_2-ZnO-BaO-Based Glasses for Mid-Infrared Transmitting Optics. *Materials* **2020**, *13*, 5829. [CrossRef]
12. Strutynski, C.; Evrard, M.; Le Gendre, A.; Maldonado, A.; Désévédavy, F.; Gadret, G.; Jules, J.-C.; Smektala, F. Physicochemical Properties and Fiber-Drawing Ability of Tellurite Glasses in the TeO_2-ZnO-Y_2O_3 Ternary System. *Materials* **2022**, *15*, 1177. [CrossRef]
13. Gunha, J.V.; Muniz, R.F.; Somer, A.; Gonçalves, A.; Denkiewicz, R.; de Souza Antero, G.; Sales, T.O.; Jacinto, C.; El-Mallawany, R.; Novatski, A. Characterization of Oxyfluorotellurite Glasses with TeO_2–Li2O–ZnO–LiF Composition. *Ceram. Int.* **2022**, *48*, 4302–4311. [CrossRef]
14. O'Donnell, M.D.; Richardson, K.; Stolen, R.; Seddon, A.B.; Furniss, D.; Tikhomirov, V.K.; Rivero, C.; Ramme, M.; Stegeman, R.; Stegeman, G.; et al. Tellurite and Fluorotellurite Glasses for Fiber optic Raman Amplifiers: Glass Characterization, Optical Properties, Raman Gain, Preliminary Fiberization, and Fiber Characterization. *J. Am. Ceram. Soc.* **2007**, *90*, 1448–1457. [CrossRef]
15. Gomes, L.; Lousteau, J.; Milanese, D.; Scarpignato, G.C.; Jackson, S.D. Energy Transfer and Energy Level Decay Processes in Tm^{3+}-Doped Tellurite Glass. *J. Appl. Phys.* **2012**, *111*, 063105. [CrossRef]
16. Yao, T.; Huang, L.; Zhou, P.; Lei, B.; Leng, J.; Chen, J. Power Scaling on Tellurite Glass Raman Fibre Lasers for Mid-Infrared Applications. *High Pow Laser Sci. Eng.* **2018**, *6*, e24. [CrossRef]
17. Plotnichenko, V.G.; Sokolov, V.O.; Koltashev, V.V.; Dianov, E.M.; Grishin, I.A.; Churbanov, M.F. Raman Band Intensities of Tellurite Glasses. *Opt. Lett.* **2005**, *30*, 1156–1158. [CrossRef] [PubMed]
18. Jauregui, C.; Limpert, J.; Tünnermann, A. High-Power Fibre Lasers. *Nat. Photon.* **2013**, *7*, 861–867. [CrossRef]
19. Zervas, M.N.; Codemard, C.A. High Power Fiber Lasers: A Review. *IEEE J. Select. Topics Quantum Electron.* **2014**, *20*, 219–241. [CrossRef]
20. Cristiani, I.; Lacava, C.; Rademacher, G.; Puttnam, B.J.; Luìs, R.S.; Antonelli, C.; Mecozzi, A.; Shtaif, M.; Cozzolino, D.; Bacco, D.; et al. Roadmap on Multimode Photonics. *J. Opt.* **2022**, *24*, 083001. [CrossRef]
21. Lin, X.-J.; Gao, Y.-X.; Long, J.-G.; Wu, J.-W.; Li, X.-Y.; Hong, W.-Y.; Cui, H.; Luo, Z.-C.; Xu, W.-C.; Luo, A.-P. Spatial Beam Self-Cleaning in Bi-Tapered Multimode Fibers. *Photonics* **2021**, *8*, 479. [CrossRef]
22. Trikshev, A.I.; Kurkov, A.S.; Tsvetkov, V.B.; Filatova, S.A.; Kertulla, J.; Filippov, V.; Chamorovskiy, Y.K.; Okhotnikov, O.G. A 160 W Single-Frequency Laser Based on an Active Tapered Double-Clad Fiber Amplifier. *Laser Phys. Lett.* **2013**, *10*, 065101. [CrossRef]
23. Khudyakov, M.M.; Levchenko, A.E.; Velmiskin, V.V.; Bobkov, K.K.; Aleshkina, S.S.; Zaushitsyna, T.S.; Bubnov, M.M.; Yashkov, M.V.; Guryanov, A.N.; Kotov, L.V.; et al. Narrow-Linewidth Diffraction-Limited Tapered Er-Doped Fiber Amplifier with 2 mJ Pulse Energy. *Photonics* **2022**, *9*, 933. [CrossRef]
24. Klenke, A.; Jauregui, C.; Steinkopff, A.; Aleshire, C.; Limpert, J. High-Power Multicore Fiber Laser Systems. *Prog. Quantum Electron.* **2022**, *84*, 100412. [CrossRef]
25. Ortiz, A.M.; Sáez, R.L. Multi-Core Optical Fibers: Theory, Applications and Opportunities. *Sel. Top. Opt. Fiber Technol. Appl.* **2018**, *2*, 63–102. [CrossRef]
26. Wolf, A.; Dostovalov, A.; Bronnikov, K.; Skvortsov, M.; Wabnitz, S.; Babin, S. Advances in Femtosecond Laser Direct Writing of Fiber Bragg Gratings in Multicore Fibers: Technology, Sensor and Laser Applications. *Opto-Electron. Adv.* **2022**, *5*, 210055. [CrossRef]
27. Agrawal, G.P. *Nonlinear Fiber Optics*, 6th ed.; Elsevier: Amsterdam, The Netherlands, 2019.
28. Balakin, A.A.; Skobelev, S.A.; Anashkina, E.A.; Andrianov, A.V.; Litvak, A.G. Coherent Propagation of Laser Beams in a Small-Sized System of Weakly Coupled Optical Light-Guides. *Phys. Rev. A* **2018**, *98*, 043857. [CrossRef]
29. Balakin, A.A.; Skobelev, S.A.; Andrianov, A.V.; Anashkina, E.A.; Litvak, A.G. Coherent Amplification of High-Power Laser Radiation in Multicore Fibers from a Rectangular Array of Cores. *Opt. Lett.* **2021**, *46*, 246–249. [CrossRef]

30. Andrianov, A.V.; Kalinin, N.A.; Anashkina, E.A.; Egorova, O.N.; Lipatov, D.S.; Kim, A.V.; Semjonov, S.L.; Litvak, A.G. Selective Excitation and Amplification of Peak-Power-Scalable Out-of-Phase Supermode in Yb-Doped Multicore Fiber. *J. Light. Technol.* **2020**, *38*, 2464–2470. [CrossRef]
31. Tünnermann, H.; Shirakawa, A. Self-Focusing in Multicore Fibers. *Opt. Express* **2015**, *23*, 2436–2445. [CrossRef]
32. Bookey, H.T.; Lousteau, J.; Jha, A.; Gayraud, N.; Thomson, R.R.; Psaila, N.D.; Li, H.; MacPherson, W.N.; Barton, J.S.; Kar, A.K. Multiple Rare Earth Emissions in a Multicore Tellurite Fiber with a Single Pump Wavelength. *Opt. Express* **2007**, *15*, 17554–17561. [CrossRef] [PubMed]
33. Cheng, T.; Duan, Z.; Gao, W.; Asano, K.; Liao, M.; Deng, D.; Suzuki, T.; Ohishi, Y. A Novel Seven-Core Multicore Tellurite Fiber. *J. Light. Technol.* **2013**, *31*, 1793–1796. [CrossRef]
34. Anashkina, E.A.; Andrianov, A.V. Design and Dispersion Control of Microstructured Multicore Tellurite Glass Fibers with In-Phase and Out-of-Phase Supermodes. *Photonics* **2021**, *8*, 113. [CrossRef]
35. Kalinin, N.A.; Anashkina, E.A.; Egorova, O.N.; Zhuravlev, S.G.; Semjonov, S.L.; Kim, A.V.; Litvak, A.G.; Andrianov, A.V. Controlled Excitation of Supermodes in a Multicore Fiber with a 5×5 Square Array of Strongly Coupled Cores. *Photonics* **2021**, *8*, 314. [CrossRef]
36. Yan, X.; Kito, C.; Miyoshi, S.; Liao, M.; Suzuki, T.; Ohishi, Y. Raman Transient Response and Enhanced Soliton Self-Frequency Shift in ZBLAN Fiber. *J. Opt. Soc. Am. B* **2012**, *29*, 238–243. [CrossRef]
37. Li, W.; Seal, S.; Rivero, C.; Lopez, C.; Richardson, K.; Pope, A.; Schulte, A.; Myneni, S.; Jain, H.; Antoine, K.; et al. Role of S/Se Ratio in Chemical Bonding of As–S–Se Glasses Investigated by Raman, x-Ray Photoelectron, and Extended x-Ray Absorption Fine Structure Spectroscopies. *J. Appl. Phys.* **2005**, *98*, 053503. [CrossRef]

Disclaimer/Publisher's Note: The statements, opinions and data contained in all publications are solely those of the individual author(s) and contributor(s) and not of MDPI and/or the editor(s). MDPI and/or the editor(s) disclaim responsibility for any injury to people or property resulting from any ideas, methods, instructions or products referred to in the content.